

Copositive criteria for a two-component dark matter model*

Xin-Xin Qi (祁鑫鑫)^{id} Hao Sun (孙昊)^{†id}

Institute of Theoretical Physics, School of Physics, Dalian University of Technology, Dalian 116024, China

Abstract: In this study, we investigate a two-component scalar dark matter framework featuring two singlet scalar fields as dark matter candidates. To ensure vacuum stability, we employ copositive criteria for the scalar potential. We analyze four distinct copositive scenarios characterized by specific negative parameter configurations using direct detection constraints. A comprehensive parameter space scan is performed under joint constraints from the observed dark matter relic density and direct detection experiments. The different signs of couplings not only correspond to different copositive criteria but also contribute to different parameter spaces caused by interference. The allowed values of quartic couplings are different for the four different cases; however, they all require the new Higgs to play a dominant role in determining dark matter relic density within the viable parameter space.

Keywords: dark matter, beyond standard model, vacuum stability

DOI: 10.1088/1674-1137/ade4b7 **CSTR:** 32044.14.ChinesePhysicsC.49103101

I. INTRODUCTION

The Standard Model (SM) of particle physics has been remarkably successful in describing fundamental particles and their interactions. However, astrophysical observations indicate the existence of dark matter (DM), which constitutes approximately 26.5% of the mass-energy content of the universe [1]. The existence of DM can be inferred from its gravitational effects on the large-scale structure of the universe; however, its particle nature remains elusive. In terms of particle physics, dark matter (DM) can be assumed to be some stable particles that carry no SM gauge group quantum number.

Weakly interacting massive particles (WIMPs) are one of the most popular and attractive DM candidates [2–4], wherein the observed DM relic density is generated via the "Freeze-out" mechanism [5]. Among the different WIMP models, the singlet scalar DM model is the simplest one, wherein a new singlet scalar as DM is introduced to the SM. The singlet scalar is stabilized by extra Z_2 symmetry, and there are only two free model parameters in the model with a DM mass and quartic coupling of DM with SM Higgs. The viable DM mass region is restricted by the Higgs invisible decay search at the LHC [6], DM relic density, direct detection constraint [7, 8], and indirect detection constraint attributed to the gamma-ray spectrum induced by DM annihilation observed at

Fermi-LAT [9, 10] and HESS [11]. This causes the resonant mass to be approximately half of the SM Higgs mass and high mass region to be larger than approximately 3 TeV [12]. Current direct detection experiments do not yield a clear signal, which imposes stringent constraints on DM-nucleon interactions and present a significant challenge for WIMP scenarios.

A possible solution to the problem is a multi-component DM model, which includes two or more DM species. In this model, one of the DM candidates has a large elastic cross-section on the nuclei; however, it forms a subdominant DM component that leads to a suppressed signal [13], causing it to escape the direct detection constraint. In addition, there is no preference to assume that there is only one DM candidate in the universe, and discussions about multi-component DM have been previously reported [14–17]. For a multi-component scalar DM model, an extra symmetry such as $Z_2 \times Z'_2$ [18], Z_5 symmetry [19–21], Z_7 symmetry [22], or other Z_N symmetry [23–25] can be considered to ensure the stability of DM particles.

When constructing a viable multi-component scalar DM model, the stability of the electroweak vacuum needs to be guaranteed. Scalar field theories suggest that the concept of vacuum stability is intricately linked to the properties of the scalar potential, particularly, its quartic

Received 9 April 2025; Accepted 9 June 2025; Published online 10 June 2025

* Hao Sun is supported by the National Natural Science Foundation of China (12075043 and 12147205). XinXin Qi is supported by the National Natural Science Foundation of China (12447162)

[†] E-mail: haosun@dlut.edu.cn



Content from this work may be used under the terms of the Creative Commons Attribution 3.0 licence. Any further distribution of this work must maintain attribution to the author(s) and the title of the work, journal citation and DOI. Article funded by SCOAP³ and published under licence by Chinese Physical Society and the Institute of High Energy Physics of the Chinese Academy of Sciences and the Institute of Modern Physics of the Chinese Academy of Sciences and IOP Publishing Ltd

couplings. A scalar potential bounded from below is a prerequisite for stable vacuum, which leads to copositive criteria. Copositive matrices are a class of matrices that are positive on non-negative vectors and provide a mathematical framework to assess the stability conditions of scalar potentials. These matrices enable deriving the necessary and sufficient analysis conditions for vacuum stability, which is essential for ensuring that the scalar potential does not lead to unphysical situations such as a vacuum that is not the global minimum of the potential.

Discussion about copositive criteria and DM have been presented in [26–31]. In this study, we consider a simple two-component scalar DM model and discuss the copositive criteria for the model. We introduce three singlet scalars S_1 , S_2 , and S_3 to the SM, where S_1 and S_2 represent DM candidates and S_3 has a non-zero vacuum expectation value. We obtain the two component scalar DM model [17] when S_3 is absent, which necessitates a large λ_{12} to evade direct detection and relic abundance constraints outside the Higgs resonance region. The introduction of S_3 leads to new annihilation channels and couplings of DM with SM Higgs. λ_{12} can be smaller to escape the direct detection constraints with the observed DM relic density constraint. The existence of S_3 contributes to the new DM annihilation processes so that a wider parameter space compared to those of DM models that involve only two singlet scalars can be obtained. A 4×4 copositive matrix of quartic couplings can be constructed in the model. The copositive criteria of a rank ≤ 3 matrix can be obtained concretely, whereas for a matrix with a higher rank, related discussions about the models are ignored because of their complexity. In this study, we analyze the copositive criteria of the model systematically. We consider eight cases of the copositive criteria for a rank 4 matrix; more complex cases can be obtained when considering the signs of the model couplings. Based on the direct detection constraint, we consider four different cases from the point of exchange symmetry for simplicity and estimate the viable parameter space within the DM relic density and direct detection constraints. The signs of the couplings can not only determine the copositive criteria but also make a difference in the cross-section of $2 \rightarrow 2$ processes related to DM annihilation into other scalars attributed to the interference effect. We randomly scan the selected parameter space and focus on quartic couplings with λ_{13} , λ_{23} , λ_{14} , and λ_{24} . The allowed values of $(|\lambda_{13}|, |\lambda_{14}|)$ are different for all four cases; however, all of them require the new Higgs to play a dominant role in determining DM relic density. Within the viable parameter space, copositive criteria place stringent constraints as long as some coupling is negative.

The rest of this manuscript is organized as follows. We present a two-component scalar DM model in Sec. II. In Sec. III, we discuss the copositivity of the symmetric matrix with eight different cases. In Sec. IV, we consider

the DM phenomenology of the model including relic density and direct detection. In Sec. V, we consider four different cases by fixing some of the quartic parameters to be negative and discuss the effect of copositive constraint on a viable parameter space satisfying the relic density and direct detection constraints. Finally, we present a summary in Sec. VI.

II. MODEL DESCRIPTION

We establish a simple two-component scalar DM model with $Z_2 \times Z'_2 \times Z''_2$ symmetry by introducing three singlet scalars $S_{1,2,3}$ into an SM model. The corresponding charges for DM particles S_1 and S_2 are $(-1, 1, 1)$ and $(1, -1, 1)$, and S_3 has a non-zero vacuum expectation value (vev) carrying the $(1, 1, -1)$ charge, while the SM particles carry a $(1, 1, 1)$ charge. Therefore, the potential part of the scalars can be given by

$$\begin{aligned} \mathcal{V} = & \frac{1}{2}M_1^2 S_1^2 + \frac{1}{2}M_2^2 S_2^2 - \frac{1}{2}\mu_3^2 S_3^2 - \mu_H^2 |H|^2 + \lambda_H |H|^4 + \frac{1}{4}\lambda_{11} S_1^4 \\ & + \frac{1}{4}\lambda_{22} S_2^4 + \frac{1}{4}\lambda_{33} S_3^4 + \lambda_{12} S_1^2 S_2^2 + \lambda_{13} S_1^2 S_3^2 \\ & + \lambda_{14} S_1^2 |H|^2 + \lambda_{23} S_2^2 S_3^2 + \lambda_{24} S_2^2 |H|^2 + \lambda_{34} S_3^2 |H|^2, \end{aligned} \quad (1)$$

where H represents the SM Higgs doublet. The Z'_2 symmetry is introduced to simplify the scalar potential in this study. Under unitarity gauge, H and S_3 can be expressed as

$$H = \begin{pmatrix} 0 \\ v_0 + h \\ \sqrt{2} \end{pmatrix}, \quad S_3 = s_3 + v_1, \quad (2)$$

where $v_0 = 246$ GeV corresponds to the electroweak symmetry breaking vev and v_1 represents the vev of S_3 . After spontaneous symmetry breaking (SSB), the masses of S_1 and S_2 can be given by

$$m_1^2 = M_1^2 + 2\lambda_{13}v_1^2 + \lambda_{14}v_0^2, m_2^2 = M_2^2 + 2\lambda_{23}v_1^2 + \lambda_{24}v_0^2. \quad (3)$$

where $m_1(m_2)$ represents the mass of $S_1(S_2)$. We have the squared mass matrix of s_3 and h with

$$\mathcal{M} = \begin{pmatrix} 2\lambda_{33}v_1^2 & \lambda_{34}v_0v_1 \\ \lambda_{34}v_0v_1 & 2\lambda_H v_0^2 \end{pmatrix}. \quad (4)$$

The physical masses of the two Higgs states h_1, h_2 are

$$\begin{aligned}
m_{h_1}^2 &= \lambda_H v_0^2 + \lambda_{33} v_1^2 - \sqrt{(\lambda_H v_0^2 - \lambda_{33} v_1^2)^2 + (\lambda_{34} v_0 v_1)^2}, \\
m_{h_2}^2 &= \lambda_H v_0^2 + \lambda_{33} v_1^2 + \sqrt{(\lambda_H v_0^2 - \lambda_{33} v_1^2)^2 + (\lambda_{34} v_0 v_1)^2}. \quad (5)
\end{aligned}$$

The mass eigenstate (h_1, h_2) and gauge eigenstate (h, s_3) can be related as

$$\begin{pmatrix} h_1 \\ h_2 \end{pmatrix} = \begin{pmatrix} \cos \theta & -\sin \theta \\ \sin \theta & \cos \theta \end{pmatrix} \begin{pmatrix} h \\ s_3 \end{pmatrix}. \quad (6)$$

where

$$\tan 2\theta = \frac{\lambda_{34} v_0 v_1}{\lambda_{33} v_1^2 - \lambda_H v_0^2}. \quad (7)$$

Furthermore, we can assume that h_1 represents the observed SM Higgs and h_2 represents the new Higgs in our model. The masses of the Higgs particles m_{h_1} and m_{h_2} can be selected as inputs, and the couplings of λ_H , λ_{33} , and λ_{34} can be given by

$$\begin{aligned}
\lambda_H &= \frac{(m_{h_1}^2 + m_{h_2}^2) - \cos 2\theta (m_{h_2}^2 - m_{h_1}^2)}{4v_0^2}, \\
\lambda_{33} &= \frac{(m_{h_1}^2 + m_{h_2}^2) + \cos 2\theta (m_{h_2}^2 - m_{h_1}^2)}{4v_1^2}, \\
\lambda_{34} &= \frac{\sin 2\theta (m_{h_2}^2 - m_{h_1}^2)}{2v_0 v_1}. \quad (8)
\end{aligned}$$

III. COPOSITIVITY OF THE SYMMETRIC MATRIX

The extended scalar field models beyond the SM can contain complicated quartic couplings, and therefore, it is important to formulate criteria that define the boundedness of the potential with the largest parameter space in terms of the vacuum stability constraint. One possible idea is constructing the quartic couplings as a pure square of the combinations of bilinear scalar fields and setting their coefficients to be non-negative. We imported the idea of copositivity of symmetric matrices in this study. In our model, the scalar potential quartic terms can be given with a symmetric matrix as

$$\mathcal{S} = \begin{pmatrix} \lambda_{11} & \lambda_{12} & \lambda_{13} & \lambda_{14} \\ & \lambda_{22} & \lambda_{23} & \lambda_{24} \\ & & \lambda_{33} & \lambda_{34} \\ & & & \lambda_{44} \end{pmatrix}. \quad (9)$$

In the following discussion, we use λ_{44} to represent λ_H for the sake of coherence. For this symmetric matrix of order four, we use eight different cases based on the sign distributions of off-diagonal elements to determine if this matrix is copositive. In these cases, all diagonal elements need to be positive as a generic condition. The eight cases are presented below [28].

- Case I: Matrix \mathcal{S} is copositive if and only if $\lambda_{ii} \geq 0$ when all off-diagonal elements are positive.

- Case II: Matrix \mathcal{S} is copositive if and only if $(\lambda_{ii}\lambda_{jj} - \lambda_{ij}^2) \geq 0$ when $\lambda_{ij} \leq 0$ and other off-diagonal elements are positive.

- Case III: Matrix \mathcal{S} is copositive if and only if $(\lambda_{ii}\lambda_{jj} - \lambda_{ij}^2) \geq 0, (\lambda_{ii}\lambda_{kk} - \lambda_{ik}^2) \geq 0$ when $\lambda_{ij}, \lambda_{ik} \leq 0$ and other off-diagonal elements are positive.

- Case IV: When $\lambda_{ij}, \lambda_{ik} \leq 0$, we need $(\lambda_{ii}\lambda_{jk} - \lambda_{ij}\lambda_{ik} + \sqrt{(\lambda_{ii}\lambda_{jj} - \lambda_{ij}^2)(\lambda_{ii}\lambda_{kk} - \lambda_{ik}^2)}) \geq 0$ to ensure that matrix \mathcal{S} is copositive.

- Case V: Matrix \mathcal{S} is copositive if and only if the following order three matrix is copositive:

$$\begin{pmatrix} \lambda_{ii} & \lambda_{ij} & \lambda_{ik} \\ & \lambda_{jj} & \lambda_{jk} \\ & & \lambda_{kk} \end{pmatrix}.$$

when $\lambda_{ij}, \lambda_{jk}, \lambda_{ik} \leq 0$ and the other off-diagonal elements are positive.

- Case VI: Matrix \mathcal{S} is copositive if the following matrix is copositive:

$$\begin{pmatrix} \lambda_{ii}\lambda_{jj} - \lambda_{ij}^2 & \lambda_{ii}\lambda_{jk} - \lambda_{ij}\lambda_{ik} & \lambda_{ii}\lambda_{jl} - \lambda_{ij}\lambda_{il} \\ & \lambda_{ii}\lambda_{kk} - \lambda_{ik}^2 & \lambda_{ii}\lambda_{kl} - \lambda_{ik}\lambda_{il} \\ & & \lambda_{ii}\lambda_{ll} - \lambda_{il}^2 \end{pmatrix}.$$

when $\lambda_{ij}, \lambda_{ik}, \lambda_{il} \leq 0$ and the other off-diagonal elements are positive.

- Case VII: The following matrix of order three should be copositive to make sure \mathcal{S} is copositive:

$$\begin{pmatrix} \lambda_{kk}(\lambda_{jj}\lambda_{ik}^2 - 2\lambda_{ij}\lambda_{ik}\lambda_{jk} + \lambda_{ii}\lambda_{jk}^2) & \lambda_{kk}(\lambda_{jj}\lambda_{ik} - \lambda_{ij}\lambda_{jk}) & \lambda_{kk}(\lambda_{ik}\lambda_{jl} - \lambda_{jk}\lambda_{il}) \\ & \lambda_{jj}\lambda_{kk} - \lambda_{jk}^2 & \lambda_{kk}\lambda_{jl} - \lambda_{jk}\lambda_{kl} \\ & & \lambda_{kk}\lambda_{ll} - \lambda_{kl}^2 \end{pmatrix}.$$

when $\lambda_{ij}, \lambda_{jk}, \lambda_{kl} \leq 0$ and other off-diagonal elements are positive.

- Case VIII: The following matrix of order three should be copositive to make sure \mathcal{S} is copositive:

$$\begin{pmatrix} \lambda_{ll}(\lambda_{ii}\lambda_{jl}^2 - 2\lambda_{ij}\lambda_{il}\lambda_{jl} + \lambda_{jj}\lambda_{il}^2) & \lambda_{ll}(\lambda_{ii}\lambda_{jl} - \lambda_{ij}\lambda_{il}) & \lambda_{ll}(\lambda_{ik}\lambda_{jl} - \lambda_{il}\lambda_{jk}) \\ & \lambda_{ii}\lambda_{ll} - \lambda_{il}^2 & \lambda_{il}\lambda_{ik} - \lambda_{il}\lambda_{kl} \\ & & \lambda_{kk}\lambda_{ll} - \lambda_{kl}^2 \end{pmatrix}.$$

when $\lambda_{ij}, \lambda_{jk}, \lambda_{kl}, \lambda_{il} \leq 0$ and other off-diagonal elements are positive.

We discuss these eight cases separately and obtain different allowed parameter spaces in terms of a theoretical constraint.

IV. DARK MATTER PHENOMENOLOGY

In our model, the two scalar DM particles are stabilized by $Z_2 \times Z'_2 \times Z''_2$ symmetry, which is related to the SM particles with Higgs-portal interactions. The observed DM relic density given by the Planck collaboration is $\Omega_{\text{DM}} h^2 = 0.1198 \pm 0.0012$ [32], and we consider DM production in our model to be generated with the “Freeze-out” mechanism. Both S_1 and S_2 contribute to DM relic density, and the Boltzmann equations for the number density of S_1 and S_2 are given as

$$\begin{aligned} \frac{dn_1}{dt} + 3Hn_1 &= -\langle\sigma v\rangle^{S_1 S_1 \rightarrow XX}(n_1^2 - \bar{n}_1^2) \\ &\quad -\langle\sigma v\rangle^{S_1 S_1 \rightarrow h_{1,2} h_{1,2}}(n_1^2 - \bar{n}_1^2) \\ &\quad -\langle\sigma v\rangle^{S_1 S_1 \rightarrow S_2 S_2}\left(n_1^2 - n_2^2 \frac{\bar{n}_1^2}{\bar{n}_2^2}\right), \\ \frac{dn_2}{dt} + 3Hn_2 &= -\langle\sigma v\rangle^{S_2 S_2 \rightarrow XX}(n_2^2 - \bar{n}_2^2) \\ &\quad -\langle\sigma v\rangle^{S_2 S_2 \rightarrow h_{1,2} h_{1,2}}(n_2^2 - \bar{n}_2^2) \\ &\quad -\langle\sigma v\rangle^{S_2 S_2 \rightarrow S_1 S_1}\left(n_2^2 - n_1^2 \frac{\bar{n}_2^2}{\bar{n}_1^2}\right). \end{aligned} \quad (10)$$

where $n_1(n_2)$ represents the number density of $S_1(S_2)$, $\bar{n}_1(\bar{n}_2)$ represents the number density in thermal equilibrium, H represents the Hubble expansion rate of the Universe, X represents SM particles, and $\langle\sigma v\rangle$ represents the thermally averaged annihilation cross section. In Fig. 1, we show the Feynman diagrams of DM annihilation processes related to new particles. Both S_1 and S_2 can be dominant in the DM relic density because of the ex-

change symmetry, which depends on the mass heirarchy between S_1 and S_2 . The lighter one is dominant because a heavy component can annihilate into the lighter component. To calculate the DM relic density numerically, we use the micrOMGEAs 5.0.6 package [33], wherein the model is implemented through the FeynRules package [34].

DM can scatter the nuclei with Higgs-mediated t-channel processes, which are constrained by the direct detection results. The effective Lagrangian related to DM-quark elastic scattering can be given by [35]

$$\mathcal{L}_{q,eff} = \sum_{S=S_1, S_2} -\frac{m_q}{2v_0} \left(\frac{C_{h_1 SS}}{m_{h_1}^2} + \frac{C_{h_2 SS}}{m_{h_2}^2} \right) SS \bar{q}q. \quad (11)$$

where $C_{h_1 SS}$ and $C_{h_2 SS}$ represent the couplings of dark matter $S_{1,2}$ with $h_{1,2}$ and

$$\begin{aligned} C_{h_1 S_1 S_1} &= -2\cos\theta\lambda_{14}v_0 + 2\sin\theta\lambda_{13}v_1, \\ C_{h_2 S_1 S_1} &= -2\sin\theta\lambda_{14}v_0 - 2\cos\theta\lambda_{13}v_1, \\ C_{h_1 S_2 S_2} &= -2\cos\theta\lambda_{24}v_0 + 2\sin\theta\lambda_{23}v_1, \\ C_{h_2 S_2 S_2} &= -2\sin\theta\lambda_{24}v_0 - 2\cos\theta\lambda_{23}v_1. \end{aligned} \quad (12)$$

The expression of the cross-section for the spin-independent DM-nucleon elastic scattering can be given as [36]

$$\begin{aligned} \sigma_{S_i N} &= \frac{m_N^4 f_N^2}{4\pi(m_N + m_i)^2} \left(\frac{C_{h_1 S_i S_i}}{m_{h_1}^2} \cos\theta + \frac{C_{h_2 S_i S_i}}{m_{h_2}^2} \sin\theta \right)^2, \\ (i &= 1, 2) \end{aligned} \quad (13)$$

where m_N represents the nucleon mass, and f_N represents the Higgs-nucleon form factor with $f_N = 0.308(18)$ based on the phenomenological and lattice-quantum chromodynamics calculations [37]. We have two DM particles in the model, and therefore, we compare the value of $\xi_i \sigma_{S_i N}$

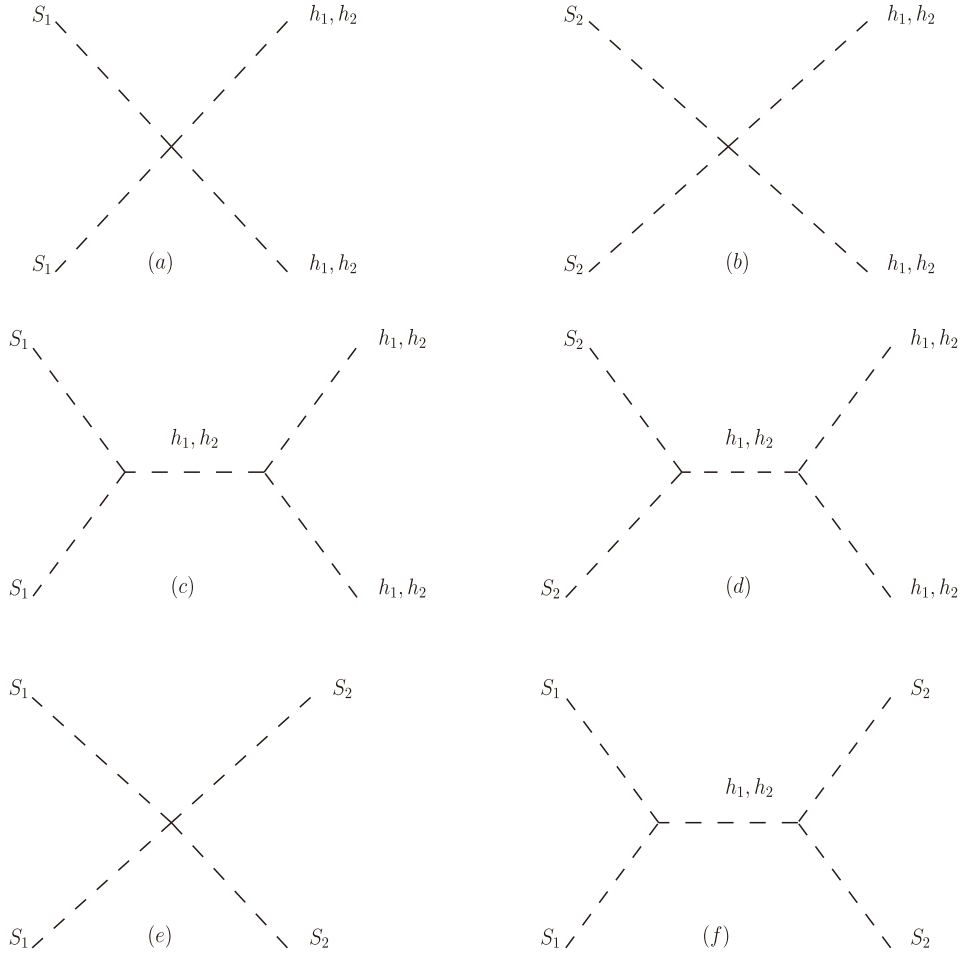


Fig. 1. Feynman diagrams of DM annihilation processes related to new particles.

against the direct detection constraints provided by the experiment results instead of the cross-section, where ξ_i represents a fraction of S_i in the total relic density defined by

$$\xi_i = \frac{\Omega_i}{\Omega_{\text{DM}}}, (i = 1, 2) \quad (14)$$

where Ω_{DM} represents the observed value of the DM density and Ω_i represents the density of S_i ($i = 1, 2$). In our analysis, we consider the current direct detection limit set by the LZ results [38].

V. DISCUSSION

We estimate the parameter space in terms of the copositive criteria and DM phenomenology related to relic density and direct detection constraints. The direct detection constraint is more stringent on the low mass region, and we focus on the TeV scale DM mass in this study, where indirect detection constraints cause slight differences on the parameter space. There are eight cases related to copositive criteria based on the sign of the para-

meters, and each case corresponds to a viable parameter space limited by the relic density constraint and direct detection constraint. Regardless of the symmetric matrix \mathcal{S} with permutation $\lambda_{ij} = \lambda_{ji}$, we can have different results when indices i, j, k , and l consider different permutations only for one case. Hence, discussions about the parameter space are complex for the different permutations of indices, and all possible cases should be considered to obtain the viable parameter space.

A. Parameter estimation

We first estimate the parameters to simplify the discussion. In this study, we select the following parameters as inputs.

$$v_1, \sin\theta, m_{h_2}, m_{1,2}, \lambda_{11}, \lambda_{12}, \lambda_{13}, \lambda_{14}, \lambda_{22}, \lambda_{23}, \lambda_{24}. \quad (15)$$

λ_{33} , λ_{34} , and $\lambda_{44}(\lambda_H)$ can be obtained from Eq. (8). λ_{34} represents the coupling of the new Higgs particles, which causes a slight difference in the DM results. Further, v_1 , $\sin\theta$, and m_{h_2} can be fixed such that λ_{33} , λ_{34} , and $\lambda_{44}(\lambda_H)$ are obtained explicitly. The self-interaction couplings λ_{11}

and λ_{22} slightly affect DM production, and we fix $\lambda_{11} = \lambda_{22} = \pi$ for the sake of simplicity. Therefore, we can just consider the signs of $\lambda_{12}, \lambda_{13}, \lambda_{23}, \lambda_{14}, \lambda_{24}$. We have an exchange symmetry of $\lambda_{13} \leftrightarrow \lambda_{23}$, $\lambda_{14} \leftrightarrow \lambda_{24}$, and $S_1 \leftrightarrow S_2$ because of the $Z_2 \times Z'_2 \times Z''_2$ symmetry, and there is no preference for the permutations of the indexes. The five couplings can be grouped as λ_{12} , $(\lambda_{13}, \lambda_{14})$, and $(\lambda_{23}, \lambda_{24})$.

The direct detection result yields the most stringent constraint on the parameter space. In Fig. 2, we obtain the viable parameter space of $(\lambda_{13}, \lambda_{14})$ satisfying the direct detection constraint with $m_1 = 1$ TeV in the absence of S_2 . In λ_{14} , the coupling of SM Higgs with S_1 is limited within a narrow region under a direct detection constraint while the value of λ_{13} is more flexible. For a heavier m_1 , a similar allowed region for $(\lambda_{13}, \lambda_{14})$ can be obtained based on the expression of DM-nucleon elastic scattering. A negative (positive) λ_{13} always demands a negative (positive) λ_{14} for a large $|\lambda_{13}|$, whereas the small values of $|\lambda_{13}|$ and $|\lambda_{14}|$ make DM production over-abundant even though the parameter space is under a direct detection constraint. Therefore, one can conclude that λ_{13} and λ_{14} consider the same signs under the direct detection constraint, which is true for λ_{23} and λ_{24} because of the exchange symmetry. Further, we are left with $7(=2^3 - 1)$ cases to be discussed, where the cases $\lambda_{12}, \lambda_{13}, \lambda_{14}, \lambda_{23}, \lambda_{24} \leq 0$ are excluded according to the copositive criteria. Owing to the exchange symmetry, the parameter space of $(\lambda_{13}, \lambda_{14})$ and $(\lambda_{23}, \lambda_{24})$ can be similar, and therefore, we can consider one case to decrease the complexity and simplify the discussion. Thus, in the following discussion, we focus on the viable parameter space of $(\lambda_{13}, \lambda_{14})$ but fix λ_{23} and λ_{24} to be constants. We discuss five cases: (1) $\lambda_{12}, \lambda_{13}, \lambda_{14}, \lambda_{23}, \lambda_{24} \geq 0$; (2) $\lambda_{12}, \lambda_{23}, \lambda_{24} \geq 0, \lambda_{13}, \lambda_{14} \leq 0$; (3) $\lambda_{12} \geq 0, \lambda_{13}, \lambda_{14}, \lambda_{23}, \lambda_{24} \leq 0$; (4) $\lambda_{12}, \lambda_{13}, \lambda_{14} \leq 0, \lambda_{23}, \lambda_{24} \geq 0$; and (5) $\lambda_{12} \leq 0, \lambda_{13}, \lambda_{14}, \lambda_{23}, \lambda_{24} \geq 0$. Case (5) always satisfies the copositive criteria because $\lambda_{11}\lambda_{22} - \lambda_{12}^2 \geq 0$ always holds, and there is no difference between Cases (1) and (5) when considering the copositive criteria. Therefore, we ignore Case (5) and focus on the first four cases.

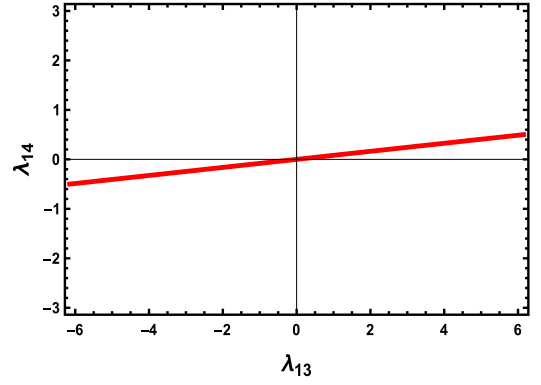


Fig. 2. (color online) Viable parameter space of $(\lambda_{13}, \lambda_{14})$ under the direct detection constraint in the absence of S_2 with $m_1 = 1$ TeV.

B. Theoretical constraint of the copositive criteria

We discuss the four different cases with the theoretical constraints of the copositive criteria. Case (1) corresponds to Case I in Sec. III where all couplings are larger than zero. Case (2) corresponds to Case IV with $\lambda_{13}, \lambda_{14} \leq 0$, and the copositive criteria demand that

$$\lambda_{11}\lambda_{34} - \lambda_{13}\lambda_{14} + \sqrt{(\lambda_{11}\lambda_{33} - \lambda_{13}^2)(\lambda_{11}\lambda_{44} - \lambda_{14}^2)} \geq 0, \quad (16)$$

Case (3) corresponds to Case VI with $\lambda_{12}, \lambda_{13}, \lambda_{14} \leq 0$, and the copositive criteria demand that

$$\lambda_{11}\lambda_{23} - \lambda_{12}\lambda_{13} + \sqrt{(\lambda_{11}\lambda_{22} - \lambda_{12}^2)(\lambda_{11}\lambda_{33} - \lambda_{13}^2)} \geq 0, \quad (17)$$

$$\lambda_{11}\lambda_{24} - \lambda_{12}\lambda_{14} + \sqrt{(\lambda_{11}\lambda_{22} - \lambda_{12}^2)(\lambda_{11}\lambda_{44} - \lambda_{14}^2)} \geq 0, \quad (18)$$

$$\lambda_{11}\lambda_{34} - \lambda_{13}\lambda_{14} + \sqrt{(\lambda_{11}\lambda_{33} - \lambda_{13}^2)(\lambda_{11}\lambda_{44} - \lambda_{14}^2)} \geq 0, \quad (19)$$

$$\begin{aligned} & \sqrt{2} \sqrt{(\lambda_{11}\lambda_{24} - \lambda_{12}\lambda_{14}) + \sqrt{(\lambda_{11}\lambda_{22} - \lambda_{12}^2)(\lambda_{11}\lambda_{44} - \lambda_{14}^2)}} \sqrt{(\lambda_{11}\lambda_{23} - \lambda_{12}\lambda_{13}) + \sqrt{(\lambda_{11}\lambda_{22} - \lambda_{12}^2)(\lambda_{11}\lambda_{33} - \lambda_{13}^2)}} \\ & \sqrt{(\lambda_{11}\lambda_{34} - \lambda_{13}\lambda_{14}) + \sqrt{(\lambda_{11}\lambda_{33} - \lambda_{13}^2)(\lambda_{11}\lambda_{44} - \lambda_{14}^2)}} + \sqrt{(\lambda_{11}\lambda_{22} - \lambda_{12}^2)(\lambda_{11}\lambda_{33} - \lambda_{13}^2)(\lambda_{11}\lambda_{44} - \lambda_{14}^2)} + (\lambda_{11}\lambda_{23} \\ & - \lambda_{12}\lambda_{13}) \sqrt{\lambda_{11}\lambda_{44} - \lambda_{14}^2} + (\lambda_{11}\lambda_{24} - \lambda_{12}\lambda_{14}) \sqrt{\lambda_{11}\lambda_{33} - \lambda_{13}^2} + (\lambda_{11}\lambda_{34} - \lambda_{13}\lambda_{14}) \sqrt{\lambda_{11}\lambda_{22} - \lambda_{12}^2} \geq 0. \end{aligned} \quad (20)$$

Case (4) belongs to Case VIII with $\lambda_{12} \geq 0, \lambda_{13}, \lambda_{14}, \lambda_{23}, \lambda_{24} \leq 0$, and we can define

$$A_{11} = \lambda_{22}(\lambda_{33}\lambda_{12}^2 - 2\lambda_{13}\lambda_{23}\lambda_{12} + \lambda_{11}\lambda_{23}^2), A_{12} = \lambda_{22}(\lambda_{33}\lambda_{12} - \lambda_{13}\lambda_{23}), A_{13} = \lambda_{22}(\lambda_{34}\lambda_{12} - \lambda_{23}\lambda_{14}),$$

$$A_{22} = \lambda_{33}\lambda_{22} - \lambda_{23}^2, A_{23} = \lambda_{22}\lambda_{34} - \lambda_{23}\lambda_{24}, A_{33} = \lambda_{44}\lambda_{22} - \lambda_{24}^2.$$

Therefore, the copositive criteria demands that

$$A_{11} \geq 0, A_{22} \geq 0, A_{33} \geq 0, A_{12} + \sqrt{A_{11}A_{22}} \geq 0, A_{13} + \sqrt{A_{11}A_{33}} \geq 0, A_{23} + \sqrt{A_{22}A_{33}} \geq 0, \quad (21)$$

$$A_{13}\sqrt{A_{22}} + A_{23}\sqrt{A_{11}} + \sqrt{2(A_{12} + \sqrt{A_{11}A_{22}})(A_{13} + \sqrt{A_{11}A_{33}})(A_{23} + \sqrt{A_{22}A_{33}})} + \sqrt{A_{11}A_{22}A_{33}} + A_{12}\sqrt{A_{33}} \geq 0. \quad (22)$$

The copositive criteria can place stringent constraints on the parameter space to obtain a stable vacuum, and different copositive criteria are expected to contribute to different viable parameter spaces that depend on the signs of quartic couplings.

C. Results

We discuss the copositive criteria, DM relic density, and direct detection constraint on the model. We consider the four different cases of the copositive criteria and focus on the viable parameter space of $(\lambda_{13}, \lambda_{14})$. We fix $v_1 = 2$ TeV, $m_{h_2} = 1.5$ TeV, and $\sin\theta = 0.01$ so that we can obtain $\lambda_{33} = 0.2812$, $\lambda_{34} = 0.0454$, and $\lambda_{44} = 0.1309$. In addition, we set $|\lambda_{12}| = 1$ and $m_2 = 3.5$ TeV and fix λ_{23} and λ_{24} as constants. We select a small $\sin\theta$ so that the contribution of $S_i S_i \rightarrow h_1 h_2 (i = 1, 2)$ is suppressed. The expression of processes related to DM production in the limit of $\sin\theta \rightarrow 0$ can be found in Appendix (A4). We randomly scan the parameter space with

$$m_1 \in \{1 \text{ TeV}, 2 \text{ TeV}, 3 \text{ TeV}\}, |\lambda_{13}| \in [0.0001, 3.14], |\lambda_{14}| \in [0.0001, 3.14].$$

In our scans, we consider the model compatible with the observed DM relic density if the value, as given by micrOMEGAs, lies between 0.119 and 0.121.

In Fig. 3, we present the results of Case (1), where we set $\lambda_{12} = 1$ and $\lambda_{13}, \lambda_{14} \geq 0$. According to Fig. 3(a), we fix $\lambda_{23} = 3.14$, $\lambda_{24} = 0.0787$, whereas in Fig. 3(b), we set $\lambda_{23} = 2.4$, $\lambda_{24} = 0.0603$. The value of λ_{24} is the upper bound obtained by the DM direct detection constraint in the absence of S_1 . The colored lines correspond to a viable parameter space of $(\lambda_{13}, \lambda_{14})$, which satisfies the relic density constraint with $m_1 = 1, 2, 3$ TeV. The respective dashed lines are the upper bound of λ_{14} arising from the direct detection constraint. The region of the colored lines below the representative dashed lines correspond to the parameter space satisfying both the relic density and direct detection constraint. The direct detection result puts the most stringent constraint on the parameter space. λ_{13} is related to processes involving h_2 , while λ_{14} is related to

processes involving SM Higgs (h_1). According to Fig. 3, when λ_{13} is small, the value of λ_{14} is approximately equal to a constant larger than 0.1 under the relic density constraint, which means the processes related to h_1 are dominant over DM production while the processes related to h_2 are less efficient. With an increase in λ_{13} , λ_{14} decrease sharply as long as λ_{13} is approximately equal to 1, where processes related to h_2 are so efficient that λ_{13} is constrained strictly and λ_{14} has a lower bound. Direct detection constraint excludes the region that λ_{13} is considerably smaller than 1, which indicates that h_2 plays an important role in determining DM production within the viable parameter space. For the heavier m_1 with $m_1 = 2$ and 3 TeV, the upper bound of λ_{13} is larger to obtain the correct relic density as the lower bound of λ_{14} is larger. However, in the case of $m_1 = 1$ TeV smaller than m_{h_2} , the process of $S_1 S_1 \rightarrow h_2 h_2$ is highly suppressed, and λ_{13} should be considerably larger to meet the relic density constraint. The lower bound of λ_{14} is larger according to Fig. 3(a). In Fig. 3(b) with $\lambda_{23} = 2.4$, $\lambda_{24} = 0.0603$, we obtain a similar conclusion, wherein the viable value of λ_{13} is at the $O(1)$ level. However, the lower bound of λ_{14} is considerably larger because the density of S_2 is larger in this case, and we require a stronger interaction related to S_1 to obtain the correct relic density.

We present the results of Case (2) in Fig. 4 with $\lambda_{12} = 1$, $\lambda_{13}, \lambda_{14} \leq 0$, where we fix (a) $\lambda_{23} = 3.14$, $\lambda_{24} = 0.0787$ and (b) $\lambda_{23} = 2.4$, $\lambda_{24} = 0.0603$. The colored lines correspond to the viable parameter space of $(|\lambda_{13}|, |\lambda_{14}|)$ satisfying a relic density constraint with $m_1 = 1, 2, 3$ TeV, and the respective dashed lines represent the upper bound of $|\lambda_{14}|$ arising from direct detection constraint. The blue-shaded region corresponds to the parameter space satisfying the copositive criteria. The cross-section of $S_i S_i \rightarrow h_i h_i (i = 1, 2)$ is determined by the Higgs-mediated processes, and therefore, the quartic term $|S_i|^2 |h_i|^2$ and t-channel processes exchange by DM, where the sign of the couplings λ_{13} and λ_{14} can create differences in the interference terms of these diagrams. Thus, the viable parameter space is different. According to Fig. 4(a), the smaller $|\lambda_{13}|$ is excluded for DM density being over-abundant because of the interference effect. Similarly, the viable

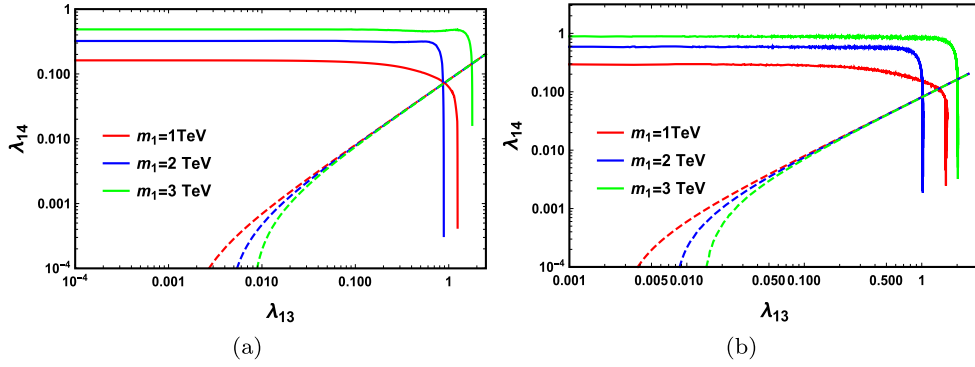


Fig. 3. (color online) Results of Case (1) with $\lambda_{12} = 1, \lambda_{13}, \lambda_{14} \geq 0$, where we fix (a) $\lambda_{23} = 3.14, \lambda_{24} = 0.0787$ and (b) $\lambda_{23} = 2.4, \lambda_{24} = 0.0603$. The colored lines correspond to the viable parameter space of $(\lambda_{13}, \lambda_{14})$ satisfying the relic density constraint with $m_1 = 1, 2, 3$ TeV, and the respective dashed lines are the upper bound of λ_{14} arising from the direct detection constraint.

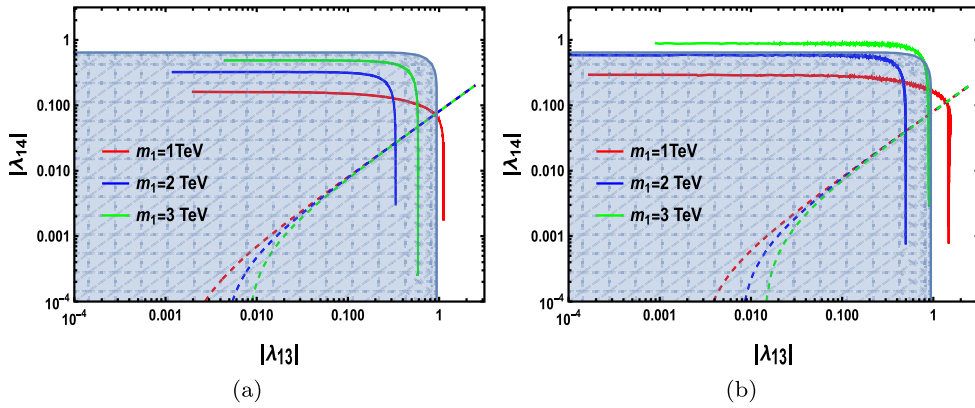


Fig. 4. (color online) Results of Case (2) with $\lambda_{12} = 1, \lambda_{13}, \lambda_{14} \leq 0$, where we fix (a) $\lambda_{23} = 3.14, \lambda_{24} = 0.0787$ and (b) $\lambda_{23} = 2.4, \lambda_{24} = 0.0603$. The blue-shadowed region corresponds to the parameter space satisfying the copositive criteria of Case (2). The colored lines correspond to the viable parameter space of $(|\lambda_{13}|, |\lambda_{14}|)$ satisfying the relic density constraint with $m_1 = 1, 2, 3$ TeV, and the respective dashed lines are the upper bound of $|\lambda_{14}|$ arising from the direct detection constraint.

$|\lambda_{13}|$ value is constrained within a narrow region while the $|\lambda_{14}|$ value is more flexible; however, it sharply decreases with an increase in $|\lambda_{13}|$ by the direct detection constraint as the results of Case (1), where h_2 plays a dominant role in determining DM production. For a larger m_1 , the upper bound of $|\lambda_{13}|$ is considerably smaller to obtain the correct relic density compared to that of the results of Case (1) in Fig. 3(a) because of the interference effect. In addition, the copositive criteria in Case (2) can constrain the parameter space strictly and for $m_1 = 1$ TeV. The allowed $(|\lambda_{13}|, |\lambda_{14}|)$ is almost excluded as shown in Fig. 4(a). For Fig. 4(b) with $\lambda_{23} = 2.4, \lambda_{24} = 0.0603$, the copositive criteria naturally exclude a small $|\lambda_{13}|$ from the point of the theoretical constraint in the case of $m_1 = 3$ TeV. Further, for $m_1 = 1$ TeV, the allowed parameter space of $(|\lambda_{13}|, |\lambda_{14}|)$ are completely excluded by the copositive criteria.

In Figs. 5(a) and (b), we present the results of Case (3) with $\lambda_{12} = -1, \lambda_{13}, \lambda_{14} \leq 0$, where we fix $\lambda_{23} = 3.14, \lambda_{24} = 0.0787$ in (a) and $\lambda_{23} = 2.4, \lambda_{24} = 0.0603$ in (b). The difference between Cases (3) and (2) is λ_{12} , set to a negative value, and the combined contribution of the Higgs-

mediated processes and quartic term $S_1^2 S_2^2$ will determine the cross-section of $S_1 S_1 \rightarrow S_2 S_2$. The sign of λ_{12} affects the interference terms; however, such interactions between S_1 and S_2 just adjust the relative relic density of S_1 and S_2 , which makes a slight difference in the viable parameter space of λ_{13} and λ_{14} . Therefore, we obtain similar results for Case (2) as we can see in Figs. 5(a) and (b).

We present the results of Case (4) in Fig. 6 with $\lambda_{12} = 1, \lambda_{13}, \lambda_{14}, \lambda_{23}, \lambda_{24} \leq 0$. The value of λ_{23} and λ_{24} are also constrained according to the copositive criteria of Case (8). Within the selected parameter space, one can obtain $|\lambda_{23}| \leq 0.94$ and $|\lambda_{24}| \leq 0.64$ with Eq. (21). In Fig. 6(a), we fix $\lambda_{23} = -0.9$ and $\lambda_{24} = -0.023$, and the allowed values of $|\lambda_{13}|$ and $|\lambda_{14}|$ are completely excluded by the direct detection constraint and copositive criteria within the selected parameter space in the case of $m_1 = 1$ TeV. For $m_1 = 3$ TeV, the allowed value of $|\lambda_{14}|$ is more flexible because of the interference effect. We set $\lambda_{23} = -0.75$ and $\lambda_{24} = -0.194$ in Fig. 6(b), where the copositive criteria exclude the parameter space of $(|\lambda_{13}|, |\lambda_{14}|)$ in the case of not only $m_1 = 1$ TeV but also $m_1 = 3$ TeV regardless of the

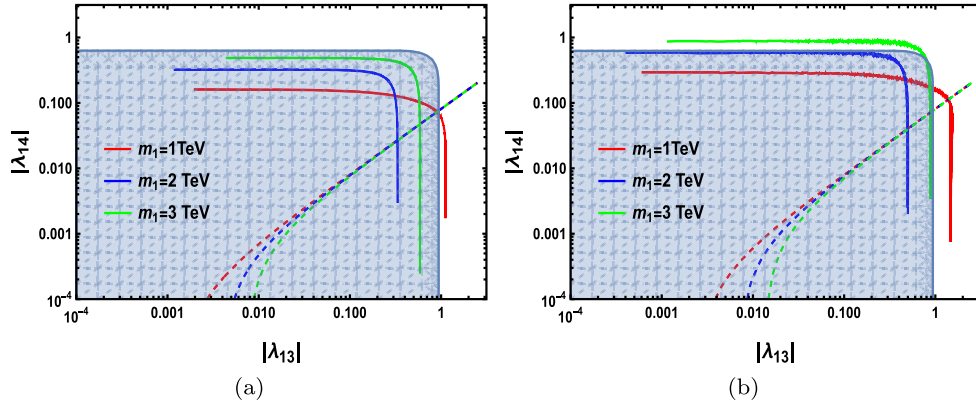


Fig. 5. (color online) Results of Case (3) with $\lambda_{12} = -1, \lambda_{13}, \lambda_{14} \leq 0$, where we fix (a) $\lambda_{23} = 3.14, \lambda_{24} = 0.0787$ and (b) $\lambda_{23} = 2.4, \lambda_{24} = 0.0603$. The blue-shadowed region corresponds to the parameter space satisfying the copositive criteria of Case (3). The colored lines correspond to the viable parameter space of $(|\lambda_{13}|, |\lambda_{14}|)$ satisfying the relic density constraint with $m_1 = 1, 2, 3$ TeV, and the respective dashed lines represent the upper bound of $|\lambda_{14}|$ arising from the direct detection constraint.

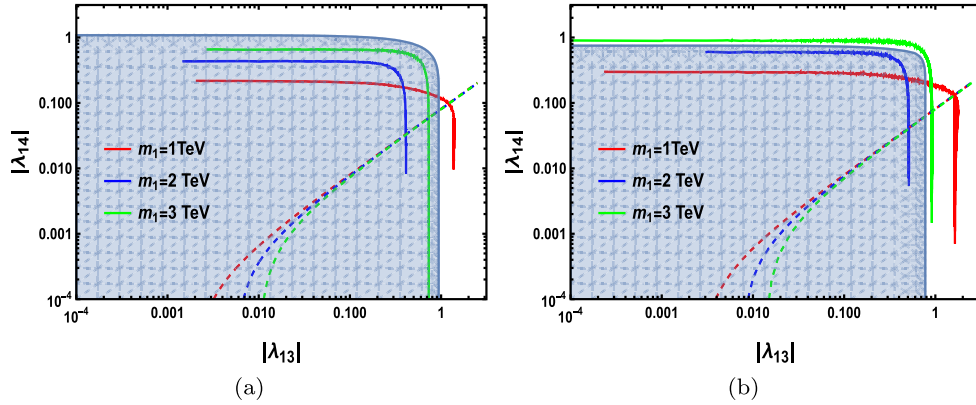


Fig. 6. (color online) Results of Case (4) with $\lambda_{12} = 1, \lambda_{13}, \lambda_{14}, \lambda_{23}, \lambda_{24} \leq 0$, where we fix (a) $\lambda_{23} = -0.9, \lambda_{24} = -0.023$ and (b) $\lambda_{23} = -0.75, \lambda_{24} = -0.194$. The blue-shadowed region corresponds to the parameter space satisfying the copositive criteria of Case (3). The colored lines correspond to the viable parameter space of $(|\lambda_{13}|, |\lambda_{14}|)$ satisfying the relic density constraint with $m_1 = 1, 2, 3$ TeV, and the respective dashed lines represent the upper bound of $|\lambda_{14}|$ arising from the direct detection constraint.

direct detection constraint.

According to Figs. 3 to 6, we show the effect of the copositive criteria on the parameter space. Different choices of the signs of couplings can contribute to different copositive conditions, which can induce different viable parameter spaces caused by the interference effect. Further, we consider four different cases and randomly scan the selected parameter space under DM relic density and direct detection constraints. Direct detection constraint places the most stringent limit on the parameter space, requiring the new Higgs h_2 to play a dominant role in determining DM relic density. The copositive criteria can also constrain the allowed parameters space such that the case of $m_1 = 1$ TeV is excluded for different copositive conditions when some of the couplings are negative. When we consider $\lambda_{12} = 1, \lambda_{13}, \lambda_{14} \leq 0, \lambda_{23} = -0.75$, and $\lambda_{24} = -0.194$, the copositive criteria are more stringent on the viable parameters, and the parameter space of $m_1 = 3$ TeV is completely excluded regardless of the direct de-

tection constraint. The high values of the couplings ~ 1 can indicate a low energy validity for the model with two stable scalars, which is expected to set limitations for the model at high energies. In the appendix, we perform a random scan and present viable parameter spaces with four different cases satisfying the copositive criteria, relic density, and direct detection constraint. According to the results, the allowed values for the couplings can be obtained at the $O(0.1)$ level, which are appropriate with a high scale validity of the model.

VI. SUMMARY AND OUTLOOK

WIMPs as DM face serious challenges in that no signals have been found in direct detection experiments so far, and therefore, one solution to such a problem is the multi-component DM model, which includes two or more DM species. The multi-component DM model is constrained by theoretical and experiment constraints. For

the extended scalar DM models, vacuum stability requires the scalar potential to be bounded from below, which can place stringent constraints on the parameter space. Further, the copositivity criteria enable deriving the necessary and sufficient analysis conditions for vacuum stability of the couplings. Different copositivity criteria can contribute to different viable parameter spaces depending on the choice of the signs of the couplings.

We considered a two-component scalar DM model in this study. The 4×4 matrix of the quadratic couplings must satisfy the copositivity criteria to obtain stable vacuum. Provided the direct detection results place stringent constraints on the parameter space, the discussion on the related parameters can indeed be simplified greatly, and we focus on four different cases related to copositivity criteria based on the signs of quadratic couplings in the model. The signs of these parameters will not only demand different copositivity criteria but also affect the results of the cross-section of the $2 \rightarrow 2$ processes and induce a different viable parameter space caused by the interference effect. We randomly scanned the selected parameter space with DM relic density and direct detection constraints. For the four different cases, the allowed values of $(|\lambda_{13}|, |\lambda_{14}|)$ are different; however, they demand the new Higgs h_2 to play a dominant role in determining the DM relic density within the viable parameter space. Further, we perform a random scan in the appendix under DM relic density and direct detection constraints; a few points "survive" when copositivity criteria are considered. For different criteria, the allowed values for the couplings are different according to the results. Thus, the copositivity criteria can place stringent constraints on the parameter space as long as some quartic coupling is negative.

The different choices of the signs of couplings can contribute to different parameter spaces with the copositivity criteria. The model in this study is simple, but the discussion about the copositivity criteria is complex because of the different permutations of the indices. For a more complex model, the copositivity enables us to find the necessary and sufficient analysis conditions to ensure vacuum stability so that the parameter space can be theoretically estimated.

APPENDIX A

1. Perturbativity

To ensure the perturbative model, the contribution from loop correction must be smaller than the tree level values, and such constraints can be ensured with

$$|\lambda_{13}| < 4\pi, |\lambda_{23}| < 4\pi, |\lambda_{12}| < 4\pi, |\lambda_{14}| < 4\pi, |\lambda_{24}| < 4\pi. \quad (A1)$$

2. Perturbativity unitarity

Unitarity conditions arise from the tree-level scalar-scalar scattering matrix, which is dominated by the quartic contact interaction. The s -wave scattering amplitudes should lie under the perturbative unitarity limit, given the requirement that the eigenvalues of the S -matrix \mathcal{M} must be less than the unitarity bound given by $|\text{Re}\mathcal{M}| < \frac{1}{2}$.

3. Renormalization group equations of quartic couplings

In this section, we present the renormalization group equations of the model with SARAH [39] at a one-loop level. The beta functions of the quartic couplings are given by

$$\begin{aligned} \beta_{\lambda_{24}} = & +2\lambda_{12}\lambda_{14} - \frac{9}{10}g_1^2\lambda_{24} - \frac{9}{2}g_2^2\lambda_{24} + 8\lambda_{22}\lambda_{24} \\ & + 4\lambda_{24}^2 + 2\lambda_{23}\lambda_{34} + 12\lambda_{24}\lambda_{44} + 6\lambda_{24}y_t^2, \end{aligned} \quad (A2)$$

$$\begin{aligned} \beta_{\lambda_{14}} = & -\frac{9}{10}g_1^2\lambda_{14} - \frac{9}{2}g_2^2\lambda_{14} + 8\lambda_{11}\lambda_{14} + 4\lambda_{14}^2 + 2\lambda_{12}\lambda_{24} \\ & + 2\lambda_{13}\lambda_{34} + 12\lambda_{14}\lambda_{44} + 6\lambda_{14}y_t^2, \end{aligned} \quad (A3)$$

$$\beta_{\lambda_{12}} = 2\lambda_{13}\lambda_{23} + 4\lambda_{12}^2 + 4\lambda_{14}\lambda_{24} + 8\lambda_{11}\lambda_{12} + 8\lambda_{12}\lambda_{22}, \quad (A4)$$

$$\beta_{\lambda_{23}} = 2\lambda_{12}\lambda_{13} + 4(2\lambda_{22}\lambda_{23} + 2\lambda_{23}\lambda_{33} + \lambda_{24}\lambda_{34} + \lambda_{23}^2), \quad (A5)$$

$$\beta_{\lambda_{13}} = 2\lambda_{12}\lambda_{23} + 4\lambda_{13}^2 + 4\lambda_{14}\lambda_{34} + 8\lambda_{11}\lambda_{13} + 8\lambda_{13}\lambda_{33}. \quad (A6)$$

where y_t represents the Top Yukawa coupling, and g_1 and g_2 represent the gauge couplings of $U(1)$ and $SU(2)$.

4. Cross section of $S_i S_i \rightarrow h_i h_i$ and $S_i S_i \rightarrow h_1 h_2$ ($i = 1, 2$)

We consider the cross section of $S_i S_i \rightarrow h_i h_i$ and $S_i S_i \rightarrow h_1 h_2$ ($i = 1, 2$) in this section. We calculate the cross section using CalcHep [40]. The expressions in the limit of $\sin\theta \rightarrow 0$ are given as

$$\sigma_{S_1 S_1 \rightarrow h_1 h_1} = \frac{\lambda_{14}^2}{8\pi s(s-4m_1^2)} \left(\sqrt{(s-4m_{h_1}^2)(s-4m_1^2)} \left(\frac{8\lambda_{14}^2 v_0^4}{m_{h_1}^4 - 4m_{h_1}^2 m_1^2 + m_1^2 s} + \frac{(2m_{h_1}^2 + s)^2}{(m_{h_1}^2 - s)^2} \right) + \frac{8\lambda_{14} v_0^2 (2\lambda_{14} v_0^2 (m_{h_1}^2 - s) - 4m_{h_1}^4 + s^2)}{2m_{h_1}^4 - 3m_{h_1}^2 s + s^2} \right. \\ \left. \times \log \left(\frac{2m_{h_1}^2 + s \left(\sqrt{\frac{(s-4m_{h_1}^2)(s-4m_1^2)}{s^2}} - 1 \right)}{2m_{h_1}^2 - s \left(\sqrt{\frac{(s-4m_1^2)(s-4m_{h_1}^2)}{s^2}} + 1 \right)} \right) \right), \quad (\text{A7})$$

$$\sigma_{S_1 S_1 \rightarrow h_2 h_2} = \frac{\lambda_{13}^2}{8\pi s(s-4m_1^2)} \left(\sqrt{(s-4m_{h_2}^2)(s-4m_1^2)} \left(\frac{8\lambda_{13}^2 v_1^4}{m_{h_2}^4 - 4m_{h_2}^2 m_1^2 + m_1^2 s} + \frac{(2m_{h_2}^2 + s)^2}{(m_{h_2}^2 - s)^2} \right) + \frac{8\lambda_{13} v_1^2 (2\lambda_{13} v_1^2 (m_{h_2}^2 - s) - 4m_{h_2}^4 + s^2)}{2m_{h_2}^4 - 3m_{h_2}^2 s + s^2} \right. \\ \left. \times \log \left(\frac{2m_{h_2}^2 + s \left(\sqrt{\frac{(s-4m_{h_2}^2)(s-4m_1^2)}{s^2}} - 1 \right)}{2m_{h_2}^2 - s \left(\sqrt{\frac{(s-4m_1^2)(s-4m_{h_2}^2)}{s^2}} + 1 \right)} \right) \right), \quad (\text{A8})$$

$$\sigma_{S_2 S_2 \rightarrow h_1 h_1} = \frac{\lambda_{24}^2}{8\pi s(s-4m_2^2)} \left(\sqrt{(s-4m_{h_1}^2)(s-4m_2^2)} \left(\frac{8\lambda_{24}^2 v_0^4}{m_{h_1}^4 - 4m_{h_1}^2 m_2^2 + m_2^2 s} + \frac{(2m_{h_1}^2 + s)^2}{(m_{h_1}^2 - s)^2} \right) + \frac{8\lambda_{24} v_0^2 (2\lambda_{24} v_0^2 (m_{h_1}^2 - s) - 4m_{h_1}^4 + s^2)}{2m_{h_1}^4 - 3m_{h_1}^2 s + s^2} \right. \\ \left. \times \log \left(\frac{2m_{h_1}^2 + s \left(\sqrt{\frac{(s-4m_{h_1}^2)(s-4m_2^2)}{s^2}} - 1 \right)}{2m_{h_1}^2 - s \left(\sqrt{\frac{(s-4m_2^2)(s-4m_{h_1}^2)}{s^2}} + 1 \right)} \right) \right), \quad (\text{A9})$$

$$\sigma_{S_2 S_2 \rightarrow h_2 h_2} = \frac{\lambda_{23}^2}{8\pi s(s-4m_2^2)} \left(\sqrt{(s-4m_{h_2}^2)(s-4m_2^2)} \left(\frac{8\lambda_{23}^2 v_1^4}{m_{h_2}^4 - 4m_{h_2}^2 m_2^2 + m_2^2 s} + \frac{(2m_{h_2}^2 + s)^2}{(m_{h_2}^2 - s)^2} \right) + \frac{8\lambda_{23} v_1^2 (2\lambda_{23} v_1^2 (m_{h_2}^2 - s) - 4m_{h_2}^4 + s^2)}{2m_{h_2}^4 - 3m_{h_2}^2 s + s^2} \right. \\ \left. \times \log \left(\frac{2m_{h_2}^2 + s \left(\sqrt{\frac{(s-4m_{h_2}^2)(s-4m_2^2)}{s^2}} - 1 \right)}{2m_{h_2}^2 - s \left(\sqrt{\frac{(s-4m_2^2)(s-4m_{h_2}^2)}{s^2}} + 1 \right)} \right) \right), \quad (\text{A10})$$

$$\sigma_{S_1 S_1 \rightarrow h_1 h_2} = \frac{4\lambda_{13}^2 \lambda_{14}^2 v_0^2 v_1^2}{\pi s(s-4m_1^2)} \frac{\log \left(\frac{m_{h_1}^2 + s \left(\sqrt{\frac{(s-4m_1^2)(m_{h_1}^4 - 2m_{h_1}^2 (m_{h_2}^2 + s) + (m_{h_2}^2 - s)^2)}{s^3}} - 1 \right) + m_{h_2}^2}{m_{h_1}^2 - s \left(\sqrt{\frac{(s-4m_1^2)(m_{h_1}^4 - 2m_{h_1}^2 (m_{h_2}^2 + s) + (m_{h_2}^2 - s)^2)}{s^3}} + 1 \right) + m_{h_2}^2} \right)}{m_{h_1}^2 + m_{h_2}^2 - s} \\ + \frac{s \sqrt{\frac{(s-4m_1^2)(m_{h_1}^4 - 2m_{h_1}^2 (m_{h_2}^2 + s) + (m_{h_2}^2 - s)^2)}{s}}}{2(-2m_1^2 s(m_{h_1}^2 + m_{h_2}^2) + m_1^2 (m_{h_1}^2 - m_{h_2}^2)^2 + m_{h_1}^2 m_{h_2}^2 s + m_1^2 s^2)}, \quad (\text{A11})$$

$$\begin{aligned}
\sigma_{S_2 S_2 \rightarrow h_1 h_2} = & \frac{4\lambda_{23}^2 \lambda_{24}^2 v_0^2 v_1^2}{\pi s(s-4m_2^2)} \frac{\log \left(\frac{m_{h_1}^2 + s \left(\sqrt{\frac{(s-4m_2^2)(m_{h_1}^4 - 2m_{h_1}^2(m_{h_2}^2 + s) + (m_{h_2}^2 - s)^2)}{s^3}} - 1 \right) + m_{h_2}^2}{m_{h_1}^2 - s \left(\sqrt{\frac{(s-4m_2^2)(m_{h_1}^4 - 2m_{h_1}^2(m_{h_2}^2 + s) + (m_{h_2}^2 - s)^2)}{s^3}} + 1 \right) + m_{h_2}^2} \right)}{m_{h_1}^2 + m_{h_2}^2 - s} \\
& + \frac{s \sqrt{\frac{(s-4m_2^2)(m_{h_1}^4 - 2m_{h_1}^2(m_{h_2}^2 + s) + (m_{h_2}^2 - s)^2)}{s}}}{2(-2m_2^2 s(m_{h_1}^2 + m_{h_2}^2) + m_2^2(m_{h_1}^2 - m_{h_2}^2)^2 + m_{h_1}^2 m_{h_2}^2 s + m_2^2 s^2)}. \quad (A12)
\end{aligned}$$

According to the expressions of the cross-section, in the limit of $\sin\theta \rightarrow 0$, the signs of λ_{13} , λ_{23} , λ_{14} , and λ_{24} can lead to differences in the terms, including the odd orders of these couplings that contribute to the cross-section of $S_i S_i \rightarrow h_i h_i (i=1,2)$. For non-zero $\sin\theta$, the signs of λ_{13} , λ_{23} , λ_{14} , and λ_{24} can lead to differences in the

cross section because of the combined contributions of these couplings such as $\lambda_{13}\lambda_{24}$.

5. Random scan results

In this section, we perform a random scan on the selected parameter space with

$$\begin{aligned}
m_{1,2} & \in [1\text{TeV}, 4\text{TeV}], |\lambda_{12}| \\
& \in [10^{-4}, 3.14], |\lambda_{13}| \in [10^{-4}, 3.14],
\end{aligned}$$

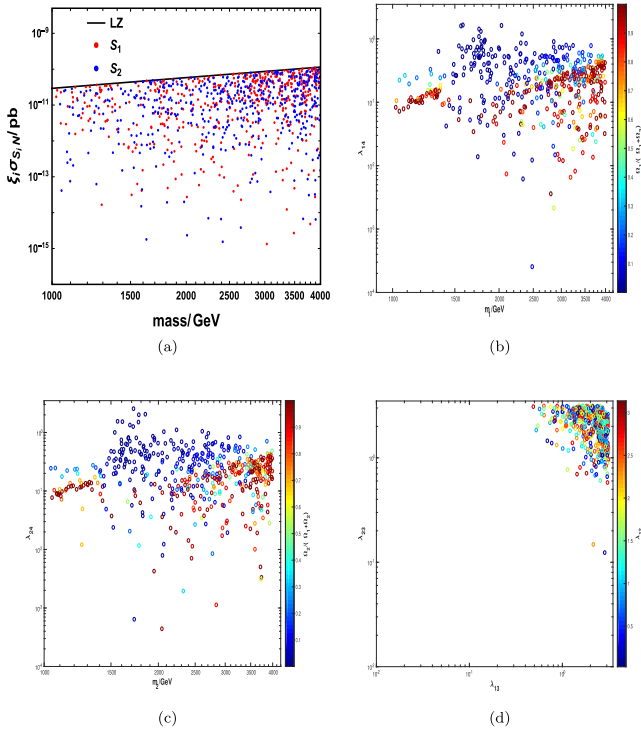


Fig. A1. (color online) Results of the viable parameter space satisfying the relic density and direct detection constraint for Case (1). (a) Allowed values for DM mass S_1 (red points) and S_2 (blue points); the black line represents the upper bound according to the latest LZ results. (b) Viable parameter space for $m_1 - \lambda_{14}$, where bubbles with different colors correspond to the fraction of S_1 defined by $\Omega_1/(\Omega_1 + \Omega_2)$. (c) Viable parameter space for $m_2 - \lambda_{24}$, where bubbles with different colors correspond to the fraction of S_2 defined by $\Omega_2/(\Omega_1 + \Omega_2)$. (d) Allowed values for $\lambda_{13} - \lambda_{23}$, where bubbles with different colors represent the viable values for λ_{12} .

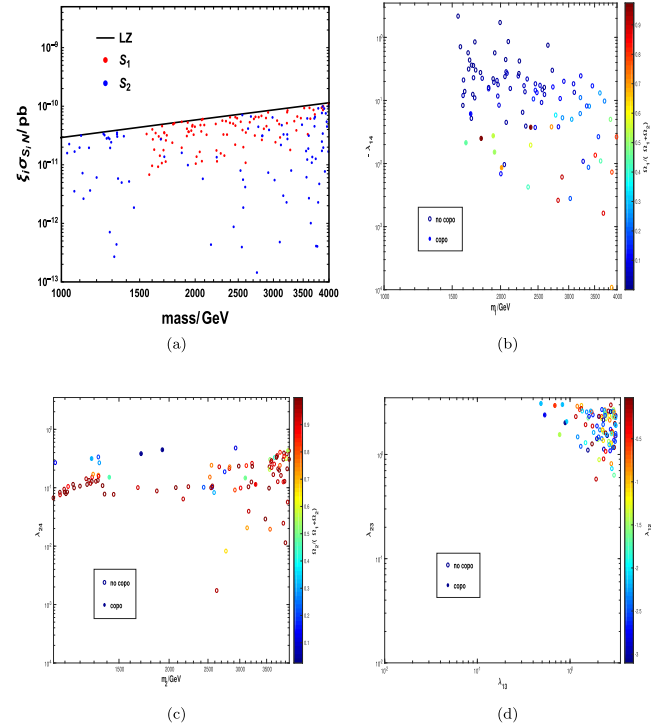


Fig. A2. (color online) Results of viable parameter space satisfying the relic density and direct detection constraint for Case (2). In (b), (c), and (d), the colored points satisfy the copositive criteria, whereas the colored bubbles do not; they are labeled as "copo" and "no copo," respectively.

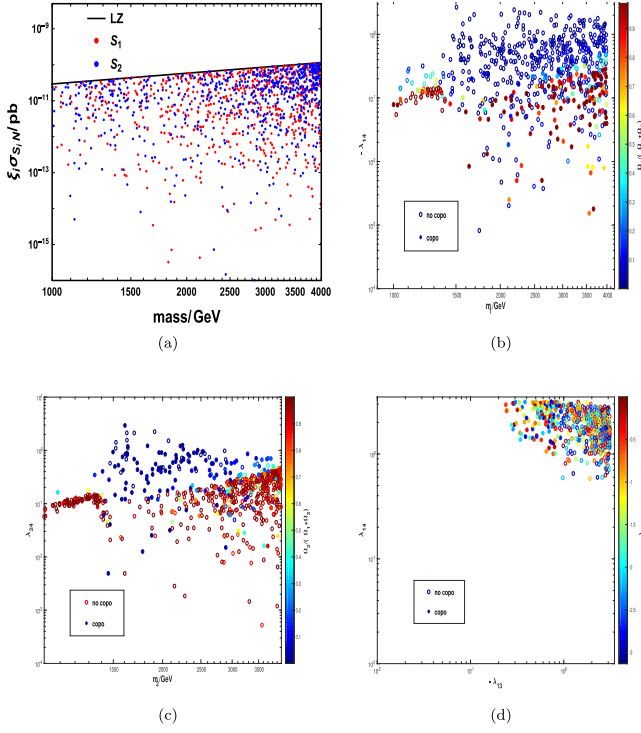


Fig. A3. (color online) Results of viable parameter space satisfying the relic density and direct detection constraint for Case (3). In (b), (c), and (d), the colored points satisfy the copositive criteria, whereas the colored bubbles do not; they are labeled as "copo" and "no copo," respectively.

$$|\lambda_{14}| \in [10^{-4}, 3.14], |\lambda_{23}| \in [10^{-4}, 3.14], |\lambda_{24}| \in [10^{-4}, 3.14].$$

We fix $\sin\theta = 0.01$, $m_{h_2} = 1.5$ TeV, and $v_1 = 2$ TeV for simplicity. We consider the copositive criteria, DM relic density, and direct detection constraint on the model for the four different cases. The results are presented in Figs. A1 to A4.

For Case (1), the copositive criteria result in a slight difference in the parameter space, and the viable parameter space satisfies the relic density and direct detection constraint as indicated in Fig. A1. Both m_1 and m_2 can have values in the range of [1 TeV, 4 TeV], as shown in Fig. A1(a). According to (b) and (c), a larger λ_{14} (λ_{24}) can contribute to a stronger interaction rate such that the fraction of S_1 (S_2) is smaller. The direct detection constraint limits λ_{14} and λ_{24} to be small, and large λ_{13} and λ_{23} are

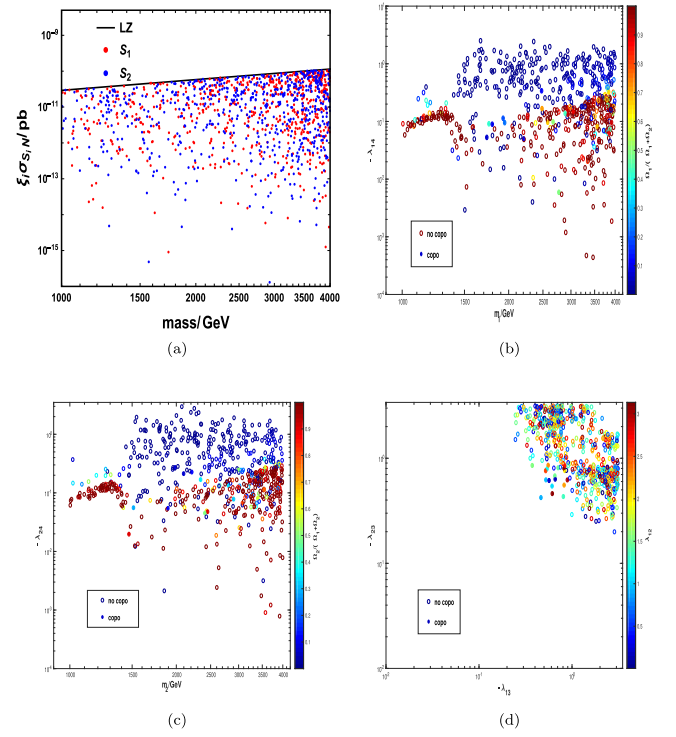


Fig. A4. (color online) Results of the viable parameter space satisfying the relic density and direct detection constraint for Case (4). In (b), (c), and (d), the colored points satisfy the copositive criteria, whereas the colored bubbles do not. They are labeled as "copo" and "no copo," respectively.

therefore required under the relic density constraint. Fig. A1(d) shows that most of the points lie in the upper right region for $(\lambda_{13}, \lambda_{23})$. In addition, λ_{12} is related to the conversion processes between S_1 and S_2 , which is less constrained.

For Cases (2), (3), and (4), we consider the copositive criteria on the parameter space. The viable parameter space satisfying the relic density and direct detection constraint is shown in Figs. A2, A3, and A4, where the colored points satisfy the copositive criteria, whereas the colored bubbles do not. They are labeled as "copo" and "no copo," respectively. We obtain a similar conclusion for Case (1); however, when considering the copositive criteria, the parameter space is more constrained, and only a few points "survive" according to Figs. A2 to A4. In addition, for the different copositive criteria, the allowed parameter spaces are different.

References

- [1] P. A. R. Ade *et al.* (Planck), *Astron. Astrophys.* **594**, A13 (2016), arXiv: 1502.01589
- [2] X. Qi, A. Yang, W. Liu *et al.*, *Chin. Phys. C* **46**, 083102 (2022), arXiv: 2106.14134
- [3] X. Qi and H. Sun, *JHEP* **09**, 118 (2023), arXiv: 2208.13345
- [4] X. Qi and H. Sun, *Phys. Rev. D* **107**, 095026 (2023b), arXiv: 2104.01045
- [5] L. Roszkowski, E. M. Sessolo, and S. Trojanowski, *Rept. Prog. Phys.* **81**, 066201 (2018), arXiv: 1707.06277
- [6] G. Aad *et al.* (ATLAS, CMS), *JHEP* **08**, 045 (2016), arXiv: 1606.02266
- [7] X. G. He and J. Tandean, *JHEP* **12**, 074 (2016), arXiv: 1606.02266

- 1609.03551
- [8] M. Escudero, A. Berlin, D. Hooper *et al.*, *JCAP* **12**, 029 (2016), arXiv: 1609.09079
- [9] M. Ackermann *et al.* (Fermi-LAT), *Phys. Rev. D* **91**, 122002 (2015a), arXiv: 1506.00013
- [10] M. Ackermann *et al.* (Fermi-LAT), *Phys. Rev. Lett.* **115**, 231301 (2015b), arXiv: 1503.02641
- [11] A. Abramowski *et al.* (H.E.S.S.), *Phys. Rev. Lett.* **110**, 041301 (2013), arXiv: 1301.1173
- [12] H. Wu and S. Zheng, *JHEP* **03**, 142 (2017), arXiv: 1610.06292
- [13] G. Belanger, A. Mjallal, and A. Pukhov, *Phys. Rev. D* **106**, 095019 (2022), arXiv: 2205.04101
- [14] B. Coleppa, K. Loho, and A. Sarkar, *Eur. Phys. J. C* **84**, 144 (2024), arXiv: 2307.14873
- [15] K. M. Zurek, *Phys. Rev. D* **79**, 115002 (2009), arXiv: 0811.4429
- [16] F. Costa, S. Khan, and J. Kim, *JHEP* **12**, 165 (2022), arXiv: 2209.13653
- [17] B. Díaz Sáez, K. Möhling, and D. Stöckinger, *JCAP* **10**, 027 (2021), arXiv: 2103.17064
- [18] S. Bhattacharya, P. Ghosh, A. K. Saha, and A. Sil, *JHEP* **03**, 090 (2020), arXiv: 1905.12583
- [19] G. Bélanger, A. Pukhov, C. E. Yaguna, and O. Zapata, *JHEP* **09**, 030 (2020), arXiv: 2006.14922
- [20] X. Qi and H. Sun (2024), arXiv: 2407.15116
- [21] X. Qi and H. Sun, *JCAP* **05**, 051 (2023), arXiv: 2303.15169
- [22] G. Bélanger, A. Pukhov, C. E. Yaguna *et al.*, *JHEP* **03**, 100 (2023), arXiv: 2212.07488
- [23] S. Bhattacharya, L. Kolay, and D. Pradhan, (2024), arXiv: 2410.16275
- [24] C. E. Yaguna and O. Zapata, *JHEP* **03**, 109 (2020), arXiv: 1911.05515
- [25] C. E. Yaguna and O. Zapata, *JHEP* **10**, 185 (2021), arXiv: 2106.11889
- [26] A. Dutta Banik, R. Roshan, and A. Sil, *Phys. Rev. D* **103**, 075001 (2021), arXiv: 2009.01262
- [27] K. Kannike, *Eur. Phys. J. C* **72**, 2093 (2012), arXiv: 1205.3781
- [28] J. Chakraborty, P. Konar, and T. Mondal, *Phys. Rev. D* **89**, 095008 (2014), arXiv: 1311.5666
- [29] A. Arhrib, R. Benbrik, M. Chabab *et al.*, *Phys. Rev. D* **84**, 095005 (2011), arXiv: 1105.1925
- [30] P. Ghorbani, *Nucl. Phys. B* **971**, 115533 (2021), arXiv: 2104.09542
- [31] Z. Habibolahi, K. Ghorbani, and P. Ghorbani, *Phys. Rev. D* **106**, 055030 (2022), arXiv: 2207.12869
- [32] G. Belanger, A. Mjallal, and A. Pukhov, *Eur. Phys. J. C* **81**, 239 (2021), arXiv: 2003.08621
- [33] G. Alguero, G. Belanger, S. Kraml *et al.*, *SciPost Phys.* **13**, 124 (2022), arXiv: 2207.10536
- [34] A. Alloul, N. D. Christensen, C. Degrande *et al.*, *Comput. Phys. Commun.* **185**, 2250 (2014), arXiv: 1310.1921
- [35] T. Basak, B. Coleppa, and K. Loho, *JHEP* **06**, 104 (2021), arXiv: 2105.09044
- [36] X. G. He, T. Li, X. Q. Li *et al.*, *Phys. Rev. D* **79**, 023521 (2009), arXiv: 0811.0658
- [37] N. F. Bell, Y. Cai, and A. D. Medina, *Phys. Rev. D* **89**, 115001 (2014), arXiv: 1311.6169
- [38] J. Aalbers *et al.* (LZ), (2024), arXiv: 2410.17036
- [39] F. Staub, *Adv. High Energy Phys.* **2015**, 840780 (2015), arXiv: 1503.04200
- [40] A. Belyaev, N. D. Christensen, and A. Pukhov, *Comput. Phys. Commun.* **184**, 1729 (2013), arXiv: 1207.6082